

Stefaan M.A. Rodts, Harm J. Jonker¹ and Peter G. Duynkerke

1. INTRODUCTION

Clouds play a key role in climate change prediction and in weather forecasting through radiative effects, latent heat release and precipitation. Cumulus is important as it couples the boundary layer to the free troposphere: cumulus transport heat, moisture, momentum, and pollutants through the inversion.

Here we first analyze aircraft observations of cumulus fields above Florida to obtain size distributions of cloud fraction, mass-flux and buoyancy flux. We compare the cloud fraction distribution with the cloud cover distribution obtained from a Landsat satellite image near the flight region. After having established which cloud sizes have the greatest impact on the vertical transport, we focuss on these clouds and present average horizontal cloud cross-sections to get more insight into the cloud dynamics.

2. DATA AND DEFINITIONS

We use data collected by the C-130 aircraft operated by the National Center for Atmospheric Research (NCAR) that participated in the Small Cumulus Microphysics Study (SCMS). The study took place from 17 July to 13 August 1995 near Cocoa Beech, Florida. Four flight days with the presence of shallow cumulus are used in our analysis: flights RF12, RF13, RF16 and RF17 on August 5, 6, 10 and 11 respectively. The flight region was 20 by 20 km; the observed clouds were quite small with typical diameters of less than 3 km. The cloud base was typically at a height of about 400 m. Cloud top was found to be around 2500 m. For a detailed description of the instrumentation on the aircraft and the accurateness of the measurements see Rodts et al. (2002).

The time spent in a single cloud multiplied by the aircraft velocity determines the cloud size. Individual clouds larger than 10 m could be detected during SCMS. All the clouds are sorted to get the cloud number density $n_1(l)$: the number of clouds with a size in the interval l and $l+dl$. The subscript 1 denotes the one-dimensional character of the aircraft measurements. The total number of observed clouds N_1 is the integral of the cloud number density.

The *cloud fraction* σ_f , here taken as the ratio of cloudy points to the total number of points, the *mass-flux* $M_c = \rho \sigma_f \overline{w'^c}$, and the *in-cloud buoyancy flux* $B_c = \sigma_f \frac{g}{\theta_0} \overline{w' \theta_v'^c}$ can be decomposed into the cloud sizes as

$$\sigma_f \equiv \int_0^\infty \alpha_f(l) dl, \quad (1)$$

¹corresponding author address: Harm Jonker, Thermal & Fluids Sciences, Delft University of Technology, Lorentzweg 1, 2628 CJ, Delft, The Netherlands
h.jonker@ws.tn.tudelft.nl

$$M_c \equiv \int_0^\infty \mu(l) dl, \quad (2)$$

$$B_c \equiv \int_0^\infty \beta(l) dl, \quad (3)$$

where the *cloud fraction density* $\alpha_f(l)$, the *mass-flux density* $\mu(l)$, and the *in-cloud buoyancy flux density* $\beta(l)$ are a function of the number density and size:

$$\alpha_f(l) \equiv \frac{1}{L} n_1(l) l, \quad (4)$$

$$\mu(l) \equiv \rho_0 \alpha_f(l) w'(l), \quad (5)$$

$$\beta(l) \equiv \frac{g}{\theta_0} \alpha_f(l) \theta_v'(l) w'(l). \quad (6)$$

with L the total flight length.

The cloud fraction density $\alpha_f(l)$ provides information on the effect of cloud size on the cloud fraction and combines the competing effects of cloud number and cloud size – bigger clouds occur less frequent but have a larger impact per cloud.

Cumulus couples the boundary layer to the free troposphere by means of transport. Both the mass-flux and the buoyancy flux are important terms in the quantification of this transport. The decompositions (4-6) provide additional information: they reveal which cloud size is most important.

We used the Landsat Thematic Mapper (TM) images from the Landsat 5 satellite with a resolution of 30 by 30 m to obtain a cloud cover distribution as a comparison for the size distributions from the flight measurements. Only high-resolution images over Florida near the flight region of the SCMS campaign of August 10 were available (the day of flight RF16) from the Landsat 5 satellite. The observed cumulus field covers an area of 65 by 65 km. The passing-by time of the satellite was 14:53 UTC.

Individual clouds are defined as the cluster of contiguous cloudy pixels. Of each individual cloud its linear size λ is calculated from the surface A of the cloud in the image

$$\lambda = \sqrt{A}, \quad (7)$$

after which the cloud number density $n(\lambda)$ is obtained. The *cloud cover* σ can be decomposed into the *cloud cover density* $\alpha(\lambda)$

$$\sigma \equiv \int_0^\infty \alpha(\lambda) d\lambda = \frac{1}{S} \int_0^\infty n(\lambda) \lambda^2 d\lambda, \quad (8)$$

which depends on the number density, the linear size and the total area of the image S .

Note that the *cloud fraction* and the *cloud cover* are intrinsic different. The cloud cover is the vertically projected area covered by clouds (satellite), whereas the cloud fraction is the area covered by clouds at a certain altitude (flights).

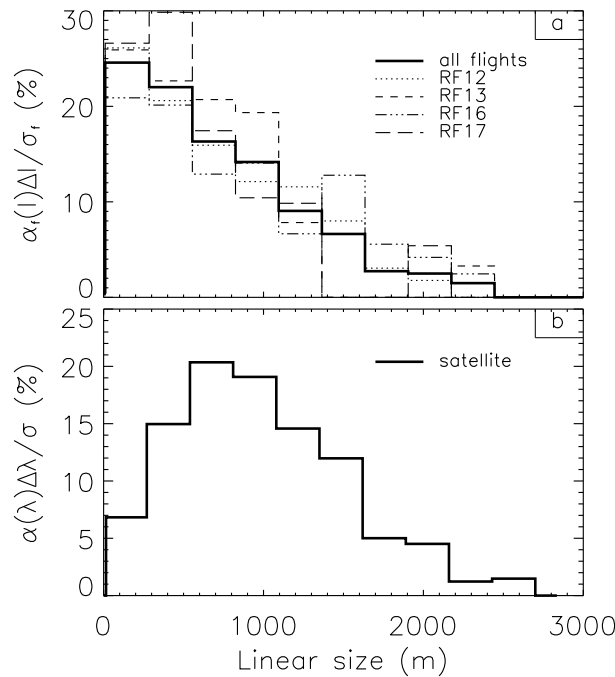


Figure 1: (a) Cloud fraction distributions obtained from four flight days during SCMS and a four-day average; (b) cloud cover distribution from Landsat 5 satellite. The bin-sizes Δl and $\Delta(\lambda)$ are 270 m.

3. SIZE DISTRIBUTIONS

Fig. 1a shows the distribution of the cloud fraction obtained from the four flights. Furthermore an average over these four days is shown. Because the aircraft flew at different heights, this density needs to be seen as an average over the cloud layer (600-2000 m).

All observed flights indicate that there is no intermediate dominating size; the cloud fraction is dominated by the smallest observed clouds (l up to 300 m). Apparently the large number of small cumuli have more effect on the cloud fraction than the size of the larger clouds. Only one flight (RF17) shows a peak in the cloud fraction density. For all other flights the peak is not visible or falls into the first bin.

The mass-flux density $\mu(l)$ and in-cloud buoyancy flux density $\beta(l)$ are shown in Fig. 2a and 2b. Whereas the cloud fraction is dominated by the smallest sized clouds, it is remarkable that the mass-flux and the in-cloud buoyancy flux – both functions of the cloud fraction – are dominated by the intermediate sized clouds. Both $\mu(l)$ and $\beta(l)$ reveal a peak near 1 km. Apparently, the intermediate sized clouds, although small in number, are the main contributors to the vertical transport. Despite the fact that the largest sized clouds individually are highly dynamic they occur too seldom to be the main contributors.

Fig. 1b shows the cloud cover distribution of the cumulus field analyzed from the Landsat image. It is surprising that the cloud cover density is dominated by an *intermediate* cloud size, as revealed by the peak at 700 m, whereas the aircraft observations indicate that the cloud fraction density

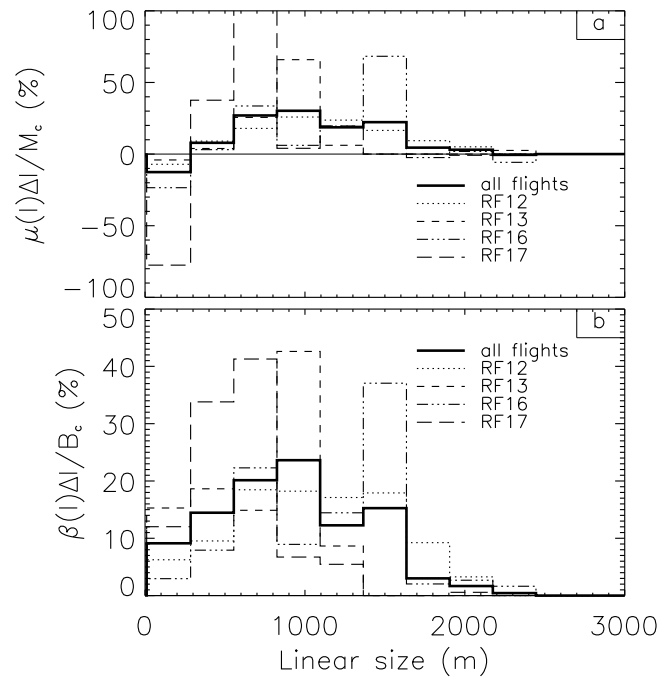


Figure 2: Size distributions obtained from four flight days during SCMS and a four-day average: (a) mass-flux density; (b) in-cloud buoyancy flux density. The bin-size Δl is 270 m.

was dominated by the *smallest* clouds in the ensemble. We therefore investigated to what extent the satellite data and aircraft data can be compared. After all, the data result from different measurement methods, the most important difference being that the aircraft data are one-dimensional and the satellite data two-dimensional.

We analytically derived an equation (Rodts et al. 2002) which couples the number densities with each other, and which enables one to translate a number density obtained from satellite data into the one-dimensional analogue, i.e. the corresponding number density as the aircraft would have observed it. To confine our analysis we neglect the third dimension (the vertical) and assume the aircraft to traverse the two-dimensional cloud field in random directions.

From stereology it is known that the total cloud fraction (or cloud cover) is independent of the dimensionality (1-D or 2-D) of the method provided that there have been an infinite number of random line measurements. If we assume the aircraft to have flown randomly and for a long period of time, we can conclude that the observed cloud fraction is representative for the real (2-D) cloud fraction. However, the flight-based cloud number *density* will generally differ from the the satellite-based number density.

If $n_2(d)$ denotes the number density of a given field of circular clouds with cloud diameters d , and $n_1(l)$ denotes the (aircraft) number density of the observed intersection lengths l , a relation can be derived to calculate the 1-D cloud number $n_1(l)$ and cloud cover density $\alpha_1(l)$ given a prescribed field of circular clouds with diameter d . The total number of clouds is N_2 ; the total number of 1-D measured

clouds is N_1 :

$$n_1(l) = \frac{N_1 l}{N_2 \bar{d}} \int_l^\infty \frac{n_2(d)}{\sqrt{d^2 - l^2}} dd, \quad (9)$$

$$\alpha_1(l) = \frac{N_1}{N_2 \bar{d}} \int_l^\infty \frac{l^2}{d^2} \frac{\alpha_2(d)}{\sqrt{d^2 - l^2}} dd, \quad (10)$$

where N_1 is the total number of clouds observed by the aircraft, N_2 the total number of clouds in the 2-D field and \bar{d} the average cloud diameter.

It is not directly clear from Eq. 10 how a 2-D dominating size translates into a 1-D dominating size for arbitrary densities n_2 . For each choice of $n_2(d)$ one would have to evaluate the integral in Eq. 10 and differentiate it with respect to l to find the 1-D dominating size. However, we would like to have a single parameter that signifies the shift in peak size independent of the prescribed cloud number density. Additional insight in the generic case can indeed be obtained by studying the so-called characteristic length scales l_c and d_c , which are defined as the first moments of $\alpha_1(l)$ and $\alpha_2(d)$ respectively. We find

$$\frac{l_c}{d_c} = \frac{8}{3\pi} \approx 0.85 \quad (11)$$

independent of the prescribed functional form of the number density $n_2(d)$. This relation implies that compared to α_2 , the 1-D cloud cover distribution α_1 will *always* be biased to smaller sizes, *irrespective* of the 2-D cloud number distribution n_2 .

The bias towards the smaller sizes is only partly explained by the methodology. In the derivation of Eq.9 we eliminated the intrinsic difference in cloud cover and cloud fraction: a 2-D cloud world, or similarity between cloud cover and cloud fraction was assumed. However effects like the 3-D shape of the cloud, wind shear, and the cloud fraying are just as important: the 2-D cloud cover density will be biased towards larger sizes, whereas at the same time the 1-D cloud fraction density is biased towards smaller sizes.

4. CROSS SECTION PROFILES

As the presented flux densities revealed that intermediate sized clouds are the main contributors to the dynamics, we investigated these clouds in more detail, focussing on the in-cloud thermodynamical structure. We produced averaged (horizontal) cross-section profiles of the vertical velocity w , the virtual potential temperature θ_v , the liquid water potential temperature θ_l and the total water content q_t in cumulus clouds with linear sizes larger than 500 m during the four flights. The restriction of 500 m assures to contain the intermediate sizes and ensures that there are enough data points per cloud. The aircraft intersected the larger clouds on average in the middle. The cross-sections thus do not say anything about cloud top or cloud base profiles. With this restriction we observed 200 clouds during the four flights. In the literature a more or less comparable study has been performed by Nicholls (1989) for downdrafts in stratocumulus and by Jonas (1990) for cumulus.

To obtain the cross-section profiles we rescaled all clouds of the four flights to unit length. All in-cloud measurement points of the observed quantity were divided into 10 equidistant bins. An equal amount of in-cloud measurement points was taken before the airplane flew into a cloud and after the airplane exited the cloud for the out-cloud regions. The average value of the region before the aircraft penetrated the cloud was subtracted from all the measured values before binning and averaging to eliminate height effects. The results are plotted on a scale of ranging from -1 to 2, where the interval $[0, 1]$ pertains to the cloudy region. Evidently, since the airplane penetrated clouds randomly, the results should be symmetric around 0.5, provided there are enough measurement points.

The results are shown in Fig. 4. The bars in the picture indicate the r.m.s. deviations from the mean and are a measure for the turbulence; they thus do not denote the error in the measurements. The variances are much higher inside the cloud than outside the cloud, as clouds are more turbulent than the environment.

On average the cloudy air parcels move upward, but just outside the cloud boundary a thin shell of air moving downward is observed. Two findings suggest that this thin shell of descending air is not due to mechanical forcing argued by Jonas (1990), but to evaporative cooling following from entrainment. In Fig. 3 these two opposing views are shown in a schematic way. Briefly, if the descending air results from mechanical forcing it will possess the properties of the air-mass at a higher level. As the total water content decreases with height, the shell is likely to have a lower value of q_t than the environment: i.e. a dip in the cross-section profile of q_t is expected. The other view, evaporative cooling resulting from entrainment, predicts a value of q_t between the environment and the cloud value, since the air in the shell is subject to strong mixing. But note that this view also predicts a significant dip in the buoyancy cross-section, because negative buoyancy is assumed to be the major driving force behind the downward motion. Such a dip is not likely for mechanical forcing, where buoyancy plays a subordinate role, and a value between cloud and environment is expected.

If we compare our observations in Fig. 4 with the schematic picture in Fig. 3, it appears the evidence in our case points to evaporative cooling due to mixing rather than to mechanical forcing as the driving mechanism of the observed descending shell of air.

5. REFERENCES

- Jonas, P. R., 1990: Observations of cumulus cloud entrainment. *Atm. Res.*, **25**, 105–127.
- Nicholls, S., 1989: The structure of radiatively driven convection in stratocumulus. *Quart. J. Roy. Meteor. Soc.*, **115**, 487–511.
- Rodts, S. M. A., P. G. Duynkerke, and H. J. J. Jonker, 2002: Size distributions and dynamical properties of shallow cumulus clouds from aircraft observations and satellite data. Submitted to *J. Atmos. Sci.*

Mechanical forcing continuity

Evaporative cooling mixing

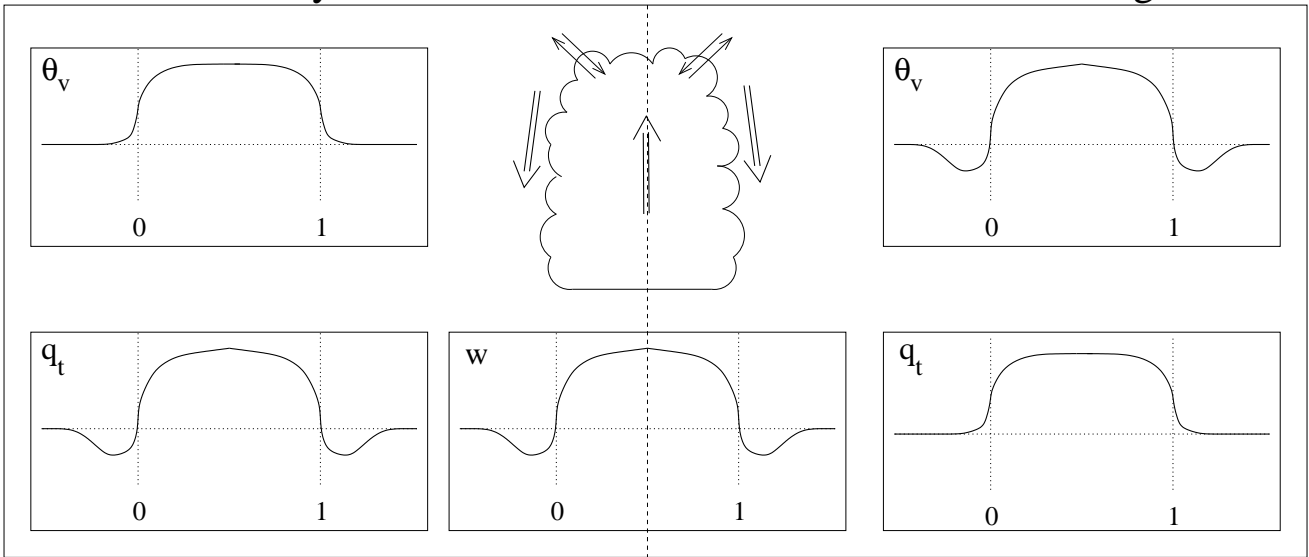


Figure 3: Schematic representation of a cloud with a descending shell of air just outside the cloud boundary and two mechanisms that can explain the descent: mechanical forcing and evaporative cooling. The averaged cross-section profiles of virtual potential temperature and total water content are depicted schematically.

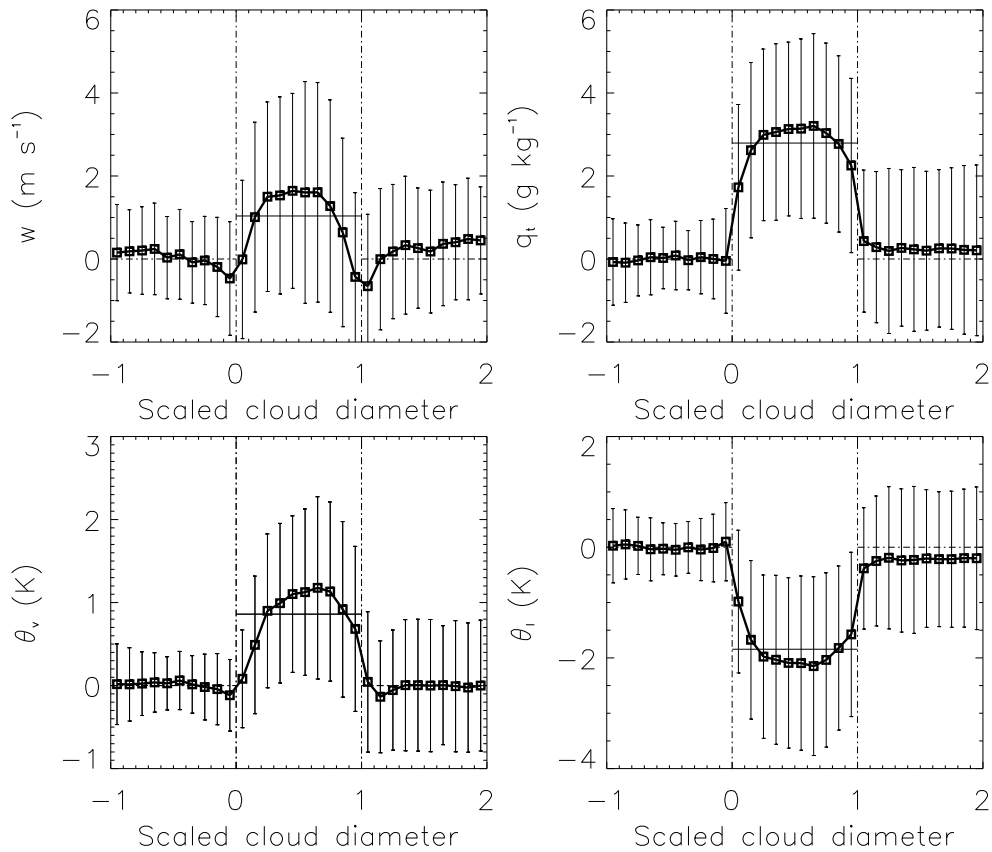


Figure 4: Average in-cloud profiles of vertical velocity, virtual potential temperature, and total water content averaged over the four flight days whereby the effect of altitude on the measurements is eliminated. The cloud region is scaled between 0 and 1. The bars denote the root mean square values of the individual measurements. These bars thus do not denote an error, but are a measure of turbulence.